Dynamic Performance Evaluation of a Redundantly Actuated and Over-constrained Parallel Manipulator

Hai-Qiang Zhang[1]　　Hai-Rong Fang[1]　　Bing-Shan Jiang[1]　　Shuai-Guo Wang[2]

[1]School of Mechanical, Electronic and Control Engineering, Beijing Jiaotong University, Beijing 100044, China

[2]MH Robot &Automation Limited Company, Weifang 262200, China

Abstract: This paper presents a redundantly actuated and over-constrained 2RPU-2SPR parallel manipulator with two rotational and one translational coupling degrees of freedom. The kinematics analysis is firstly carried out and the mapping relationship of the velocity, acceleration and the independent parameters between the actuator joint and the moving platform are deduced by using the vector dot product and cross product operation. By employing d′Alembert′s principle and the principle of virtual work, the dynamics equilibrium equation is derived, and the simplified dynamics mathematical model of the parallel manipulator is further derived. Simultaneously, the generalized inertia matrix which can characterize the acceleration performance between joint space and operation space is further separated, and the performance indices including the dynamics dexterity, inertia coupling characteristics, energy transmission efficiency and driving force/torque balance are introduced. The analysis results show that the proposed redundantly actuated and over-constrained 2RPU-2SPR parallel manipulator in comparison with the existing non-redundant one has better dynamic comprehensive performance, which can be demonstrated practically by the successful application of the parallel kinematic machine head module of the hybrid machine tool.

Keywords: Redundantly actuated, over-constrained, parallel manipulator, dynamics, performance index.

1 Introduction

Parallel manipulator has many advantages such as high stiffness, lower inertia and good dynamic characteristics. It has more obvious advantages than serial ones in speed, precision and carrying capacity in manufacturing and industrial applications[1]. To address the specific task requirement, the lower mobility parallel manipulators have been made as a plug and play parallel module, which has good reconfigurable capacity and can be utilized to construct the machining unit of high-grade hybrid kinematic machine tools or intelligent equipment system. Therefore, parallel manipulators are promising and potential candidates for advanced robotics applications. At present, the most successful application examples are Tricept machine tool[2], Exechon machine tool[3] and Sprint Z3 parallel spindle head[4], and the three degrees of freedom parallel manipulator with two rotational degrees of freedom and one translational degree of freedom has become one of the hottest focus in the mechanism field in recent years[5]. Zhang et al.[6] divided the spatial 1T2R parallel manipulators into three categories according to the rotating axis distribution property, namely, PRR configuration, RRP configuration and RPR configuration (P

is a prismatic joint, and R is a revolute joint).

The dynamics modeling of the parallel manipulator is to investigate the mapping relationship between end-effector force and the actuator driving force, which is the kernel issue of the structural design and optimization, the dynamics performance evaluation, the driving system selection and the real-time control. Due to the closed loop characteristics of the parallel mechanism, the dynamics has the features of multi-degree of freedom, multi-variable, high nonlinearity and multi-parameter coupling. Nowadays, the common methods of dynamics modeling include the principle of virtual work[7–9], the Lagrange method[10–12], the Newton-Euler method[13–15] and Kane formulation[16], etc. The dynamics performance evaluation is vitally important technical index for evaluating the advantages or disadvantages of the parallel manipulator. Bearing this in mind, Yoshikawa[17] defined the singular value of the acceleration mapping matrix between driving joint and operation space as the dynamics manipulability ellipsoid (DME), which can be employed as an index to evaluate the dynamics performance, and the smaller values of the dynamics performance are desirable. Asada[18] put forward the concept of generalized inertia ellipsoid (GIE) and considered the influence of acceleration term on the principal axis of the generalized inertial ellipsoid in dynamics formulation. More recently, Wu et al.[19] conducted the dynamics performance evaluation about three degrees of freedom parallel manipulator applied to the automobile spraying equipment, and pro-

posed the maximum and minimum singular value of the acceleration coefficient matrix to evaluate the acceleration performance and isotropy performance. Cui et al.[20] considered the transmission performance and acceleration performance of the three rotational degrees of freedom parallel manipulator, and the dynamics dexterity analysis was accomplished numerically. Zhang et al.[21] established the modal and natural frequency analysis of the 3-RPS parallel manipulator in terms of the eigenvalue decomposition of the inertial matrix to evaluate the dynamics performance. Lu and Li[22] established the general expression of the dynamics model of the 3-PUU parallel manipulator based on the principle of virtual work, and utilized the condition number of the inertia matrix as the capability index for evaluating dynamics dexterity. Li et al.[23] proposed a local and global index to evaluate the dynamics performance, and compared the performance index of two common parallel manipulators, i.e., Tricept and Trivariant. Zhao[24] derived the dynamics model considering the isotropic characteristics of three translational degrees of freedom, put forward the driving force/torque index, and further conducted the multi-objective optimization design. Wu et al.[25] formulated the dynamics modeling method about redundantly actuated and non-redundantly actuated parallel manipulator based on the principle of virtual work, and the optimal driving force is determined by the Moore-Penrose matrix. Zhao et al.[26] conducted the dynamics modeling of three degrees of freedom parallel kinematic machine (PKM) on the basis of the inverse kinematics and velocity and acceleration analysis, and verified the correctness of theoretical solution according to the desired trajectory. Chen et al.[27] utilized the vector method to deduce the velocity and acceleration of each component and solve the Jacobian matrix of each limb. The authors adopted the principle of virtual work to establish the dynamics modeling of two rotational and one translational degrees of freedom 3-UPU parallel manipulator. Jiang et al.[28] established the dynamics modeling of the novel redundantly actuated parallel manipulator applied in the parallel kinematic machine tool, and improved the accuracy of the machine by adopting redundant actuation. In practical engineering application, the dynamics performance and dynamics response characteristics of the mechanism should be synthetically evaluated according to the influence of various factors such as component quality, rotational inertia, gravity, velocity, acceleration, etc.

The rest of this paper is organized as follows. Section 1 provides the introduction. Section 2 presents the kinematic analysis and coordinate frame assignation. Dynamic analysis is carried out through the principle of virtual work in Section 3. Section 4 introduces some performance evaluation indices. Some application examples concerning the novel redundantly actuated and over-constrained 2RPU-2SPR parallel manipulator are derived in Section 5. Finally, the conclusions are presented in Section 6.

2 Kinematics analysis

2.1 Architecture description and coordinate system setting

The redundantly actuated and over-constrained parallel manipulator (as shown in Fig. 1) is composed of the base, the moving platform, four driving branches connecting the base and moving platform, and end-effector, in which the limb 1 and limb 3 form RPU configuration kinematic chain (U denotes a universal joint), the lower end is connected to the base by the rotational joint and the upper end is connected to the moving platform through the universal joint, while the limb 2 and limb 4 is SPR configuration kinematic chain (S denotes a spherical joint), the lower end is connected to the moving platform through compound spherical joint, and the upper end is connected to the moving platform through the rotational joint. The moving platform and the base are a square layout, and its circumcircle radii are r_a and r_b, respectively. The kinematic joints configuration arrangement satisfied certain geometric constraints, and the moving platform will own three degrees of freedom, namely, one translation and two rotations[29, 30]. The spatial parallel manipulator module is a good candidate for engineering application, furthermore, it can connect X-Y linear guide or ring rail in series to achieve five-axis machine tool, which can complete the complex special-shaded surface free machining.
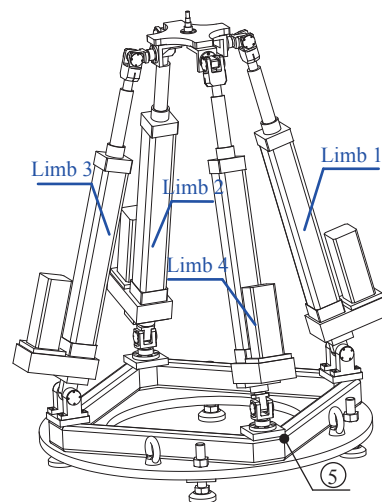
Fig. 1   A 3D model of the parallel manipulator

To facilitate analysis, the fixed coordinate system B-xyz is attached to the base platform, whose coordinate origin B is a square center of the circle, in which the x and y axes are the same as the vector BB_1 and BB_4, and the z axis is determined by the right hand rule. The relative coordinate system A-uvw is set up similarly at the moving platform. The coordinate origin A is the geometric center of the moving platform, the u and v axes are

the same as the vector AA_1 and AA_4, and the w axis is determined by the right hand rule. In addition, the chain local coordinate system B_i-$x_iy_iz_i$ $(i=1, 2, 3, 4)$ is connected to each limb joint, the origin of the coordinate system is at the B_i joint, the z_i axis points from B_i to A_i, the y_i $(i=1, 3)$ axis coincides with the rotation axis of the rotational joint, while y_i $(i=2, 4)$ coincides with the second axis of the compound spherical joint, and the x_i axis is determined by the right hand rule.

2.2 Position analysis

The pose coordinate transformation matrix T of the redundantly actuated and over-constrained parallel manipulator is obtained through three times complex transformation, i.e., rotate α around x axis, move d along new z axis, and then rotate β around v axis of the moving platform. Its position can be represented by position vector $\boldsymbol{p} \begin{pmatrix} x & y & z \end{pmatrix}$ and rotation matrix ${}^B\boldsymbol{R}_A$, and the homogeneous coordinate transformation matrix can be written as

$$\boldsymbol{T} = \begin{bmatrix} {}^B\boldsymbol{R}_A & \boldsymbol{p} \\ 0 & 1 \end{bmatrix} = Rot(x, \alpha)Trans(z, d)Rot(v, \beta) = \begin{bmatrix} c\beta & 0 & s\beta & 0 \\ s\alpha s\beta & c\alpha & -s\alpha c\beta & -ds\alpha \\ -s\beta c\alpha & s\alpha & c\alpha c\beta & dc\alpha \\ 0 & 0 & 0 & 1 \end{bmatrix} \tag{1}$$

where s and c are the abbreviations of sine and cosine functions, respectively.

$$\begin{cases} x = 0 \\ y = -ds\alpha \\ z = ds\alpha. \end{cases} \tag{2}$$

Equation (3) is the parasitic motion of the parallel manipulator through further derivation:

$$y = -z\tan\alpha. \tag{3}$$

It can be seen from (2) that the position vector $\boldsymbol{p} = \begin{bmatrix} x & y & z \end{bmatrix}^{\mathrm{T}}$ of the moving platform is a function of α, β, z, so the linear velocity $\boldsymbol{v}_p$ and angular velocity ω_p of the mechanism can be expressed by the independent variables $\boldsymbol{v}_s = \begin{bmatrix} \dot{\alpha} & \dot{\beta} & \dot{z} \end{bmatrix}^{\mathrm{T}}$

$$\boldsymbol{v}_p = \begin{bmatrix} \dfrac{\partial x}{\partial \alpha} & \dfrac{\partial x}{\partial \beta} & \dfrac{\partial x}{\partial z} \\ \dfrac{\partial y}{\partial \alpha} & \dfrac{\partial y}{\partial \beta} & \dfrac{\partial y}{\partial z} \\ \dfrac{\partial z}{\partial \alpha} & \dfrac{\partial z}{\partial \beta} & \dfrac{\partial z}{\partial z} \end{bmatrix} \begin{bmatrix} \dot{\alpha} \\ \dot{\beta} \\ \dot{z} \end{bmatrix} = \boldsymbol{J}_{vp} \begin{bmatrix} \dot{\alpha} \\ \dot{\beta} \\ \dot{z} \end{bmatrix} \tag{4}$$

where

$$\boldsymbol{J}_{vp} = \begin{bmatrix} 0 & 0 & 0 \\ -z\sec^2\alpha & 0 & -\tan\alpha \\ 0 & 0 & 1 \end{bmatrix}.$$

The angular velocity of the mechanism can be expressed as a linear superposition of the Euler angles:

$$\omega_p = Rot(\alpha)\dot{\alpha} + \boldsymbol{0}\dot{z} + Rot(\beta)\dot{\beta} = \boldsymbol{J}_{wp} \begin{bmatrix} \dot{\alpha} \\ \dot{\beta} \\ \dot{z} \end{bmatrix} \tag{5}$$

where

$$\boldsymbol{J}_{wp} = \begin{bmatrix} 1 & 0 & 0 \\ 0 & c\alpha & 0 \\ 0 & s\alpha & 0 \end{bmatrix}.$$

Therefore, the mapping relationship between generalized velocity and the independent parameter velocity can be expressed as

$$\dot{\boldsymbol{q}} = \begin{bmatrix} \boldsymbol{v}_p \\ \omega_p \end{bmatrix} = \begin{bmatrix} \boldsymbol{J}_{vp} \\ \boldsymbol{J}_{wp} \end{bmatrix} \boldsymbol{v}_s = \boldsymbol{J}_p \boldsymbol{v}_s \tag{6}$$

where $\boldsymbol{J}_p$ is the Jacobian matrix of the moving platform.

Fig. 2 shows the structural diagram of the parallel manipulator, where we can see that the closed vector constraint equation of the chain can be expressed in the fixed coordinate system:

$$\boldsymbol{b}_i + d_i\boldsymbol{s}_i = \boldsymbol{p} + \boldsymbol{a}_i. \tag{7}$$

In (7), $\boldsymbol{b}_i$ is the description of the position vector in the fixed coordinate system, and ${}^A\boldsymbol{a}_i$ is the description of the position vector in the relative coordinate system, and $\boldsymbol{a}_i$ is the representation of vector ${}^A\boldsymbol{a}_i$ in the fixed coordinate system, namely $\boldsymbol{a}_i = \boldsymbol{R} \cdot {}^A\boldsymbol{a}_i$.

The position inverse solution can be derived by
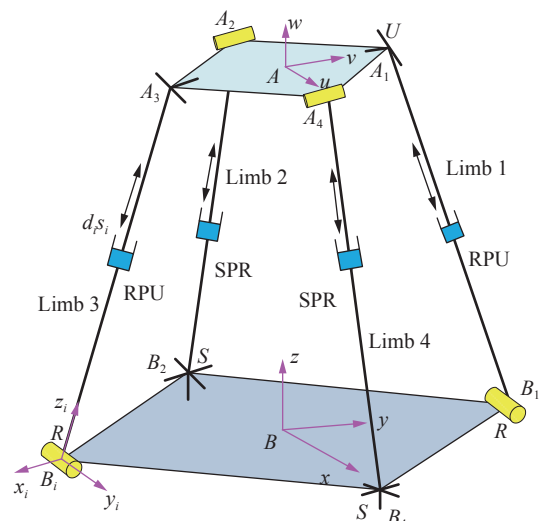
Fig. 2   Schematic of the parallel manipulator

$$d_i = \|\boldsymbol{p} + \boldsymbol{a}_i - \boldsymbol{b}_i\| \tag{8}$$

where $\|\cdot\|$ represents the 2-norm of a vector, thus

$$s_i = \frac{\|\boldsymbol{p} + \boldsymbol{a}_i - \boldsymbol{b}_i\|}{d_i}. \tag{9}$$

The chain local coordinate system can be obtained by the rotation transformation of the fixed coordinate system by the two Euler angles, i.e., rotate γ_i around z_i axis, then rotate θ_i around y_i axis resulting in the coordinate system $B_i\text{-}x_iy_iz_i$, and then the rotation matrix $^B\boldsymbol{R}_i$ of the chain coordinate system relative to the fixed coordinate system can be obtained as

$$^B\boldsymbol{R}_i = Rot(\gamma_i, z_i)Rot(y_i, \theta_i) =$$
$$\begin{bmatrix} c\gamma_i c\theta_i & -s\gamma_i & c\gamma_i s\theta_i \\ c\theta_i s\gamma_i & c\gamma_i & s\gamma_i s\theta_i \\ -s\theta_i & 0 & c\theta_i \end{bmatrix}. \tag{10}$$

It is noteworthy that the chain i ($i=1, 3$) can only rotate around $\boldsymbol{y}_i$ axis, so γ_i is a constant value, namely $\gamma_1 = \frac{\pi}{2}$, $\gamma_3 = \frac{3\pi}{2}$.

The chain unit vector s_i is expressed as ^is_i in the local coordinate system, namely $^i\boldsymbol{s}_i = \begin{bmatrix} 0 & 0 & 1 \end{bmatrix}^T$

$$\boldsymbol{s}_i = {^B\boldsymbol{R}_i} \cdot {^i\boldsymbol{s}_i} = \begin{bmatrix} c\gamma_i s\theta_i & s\gamma_i s\theta_i & c\theta_i \end{bmatrix}^T. \tag{11}$$

Through simplification and solving of (11), γ_i and θ_i can be readily obtained as

$$\begin{aligned} c\theta_i &= s_{iz}, \quad s\theta_i = \sqrt{s_{ix}{}^2 + s_{iy}{}^2}, \quad 0 \le \theta \le \pi \\ c\gamma_i &= \frac{s_{ix}}{s\theta_i}, \quad s\gamma_i = \frac{s_{iy}}{s\theta_i} \end{aligned} \tag{12}$$

where s_{ix}, s_{iy}, s_{iz} are the components $\boldsymbol{s}_i$ of x, y, z, respectively, and once the location parameters of the moving platform are given, the unit vector and Euler angles of the chains can be determined by (11) and (12).

The structural diagram of the chain i is shown in Fig. 3, each of that consists of a swing rod and a telescopic rod. Let e_1 be the distance between the centroid B_i and the center of mass of the swing rod, while e_2 be the distance of the centroid A_i and the center of mass of the telescopic rod. The position vector of the centroid of the swing rod and the centroid of the telescopic rod in the fixed coordinate system can be written as

$$\boldsymbol{r}_{1i} = \boldsymbol{b}_i + e_1\boldsymbol{s}_i \tag{13}$$

$$\boldsymbol{r}_{2i} = \boldsymbol{b}_i + (d_i - e_2)\boldsymbol{s}_i. \tag{14}$$

2.3 Velocity analysis

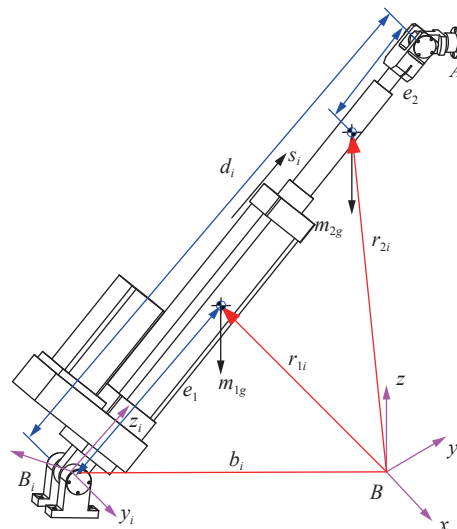The inverse kinematics (7) should be differentiated with respect to time, and the velocity of kinematic joints

Fig. 3   Structure diagram of the chain

A_i connected to the moving platform can be obtained in the fixed coordinate system:

$$\boldsymbol{v}_{ai} = \boldsymbol{v}_p + \omega_p \times \boldsymbol{a}_i = \boldsymbol{J}_{ai}\dot{\boldsymbol{q}} \tag{15}$$

where $\boldsymbol{v}_p$ and ω_p are the velocity and angular velocity of the center of the moving platform, respectively. Furthermore, we can obtain the following

$$\boldsymbol{J}_{ai} = \begin{bmatrix} 1 & 0 & 0 & 0 & a_{iz} & -a_{iy} \\ 0 & 1 & 0 & -a_{iz} & 0 & a_{ix} \\ 0 & 0 & 1 & a_{iy} & -a_{ix} & 0 \end{bmatrix}. \tag{16}$$

The active prismatic joint velocity $\dot{d}_i$ along the actuation $\boldsymbol{s}_i$ can be expressed as

$$\dot{d}_i = \boldsymbol{s}_i{}^T \cdot \boldsymbol{v}_{ai} = \boldsymbol{s}_i{}^T \cdot (\boldsymbol{v}_p + \omega_p \times \boldsymbol{a}_i) = \boldsymbol{J}_{di}\dot{\boldsymbol{q}}. \tag{17}$$

By rewriting (17) in the matrix format, we get

$$\boldsymbol{J}_{di} = \begin{pmatrix} \boldsymbol{s}_i{}^T & (\boldsymbol{a}_i \times \boldsymbol{s}_i)^T \end{pmatrix}. \tag{18}$$

The velocity of the centroid of the kinematic joints connecting the moving platform can be also obtained by taking the time derivative of (7):

$$\boldsymbol{v}_{ai} = \dot{d}_i \cdot \boldsymbol{s}_i + d_i \cdot (\omega_i \times \boldsymbol{s}_i) \tag{19}$$

where ω_i is the angular velocity of the chain i in the fixed coordinate system.

By taking the cross product of both sides of (19), we can obtain the angular velocity of the chain i:

$$\omega_i = \frac{\boldsymbol{s}_i \times \boldsymbol{v}_{ai}}{d_i} = \boldsymbol{J}_{wi}\dot{\boldsymbol{q}} \tag{20}$$

where $\boldsymbol{J}_{wi} = \dfrac{\tilde{\boldsymbol{s}}_i \boldsymbol{J}_{ai}}{d_i}$, and $\tilde{\boldsymbol{s}}_i$ is anti-symmetric operator

corresponding to the vector $\boldsymbol{s}_i$.

$$\tilde{\boldsymbol{s}}_i = \begin{bmatrix} 0 & -s_{iz} & s_{iy} \\ s_{iz} & 0 & -s_{ix} \\ -s_{iy} & s_{ix} & 0 \end{bmatrix}. \qquad (21)$$

Taking the derivative of (13) and (14) with respect to time, the velocity of the center of mass of the swing rod and telescopic rod can be obtained in the fixed coordinate system.

$$\boldsymbol{v}_{1i} = e_1 \omega_i \times \boldsymbol{s}_i = \boldsymbol{J}_{v1} \dot{\boldsymbol{q}} \qquad (22)$$

where $\boldsymbol{J}_{v1i} = -e_1 \cdot \tilde{\boldsymbol{s}}_i \boldsymbol{J}_{wi}$

$$\boldsymbol{v}_{2i} = (d_i - e_2)\omega_i \times \boldsymbol{s}_i + \dot{d}_i \cdot \boldsymbol{s}_i = \boldsymbol{J}_{v2} \dot{\boldsymbol{q}} \qquad (23)$$

and $\boldsymbol{J}_{v2i} = (e_2 - d_i) \cdot \tilde{\boldsymbol{s}}_i \boldsymbol{J}_{wi} + \boldsymbol{s}_i \boldsymbol{J}_{di}$.

Combining (20), (22) and (23) yields

$$\boldsymbol{J}_{v\omega1i} = \begin{bmatrix} \boldsymbol{J}_{v1i} \\ \boldsymbol{J}_{wi} \end{bmatrix}, \quad \boldsymbol{J}_{v\omega2i} = \begin{bmatrix} \boldsymbol{J}_{v2i} \\ \boldsymbol{J}_{wi} \end{bmatrix} \qquad (24)$$

where $\boldsymbol{J}_{v\omega1i}$ and $\boldsymbol{J}_{v\omega2i}$ are the generalized Jacobian matrices of the chain i.

2.4 Acceleration analysis

Taking the derivative of (15) with respect to time, the acceleration of the point A_i can be obtained as

$$\dot{v}_{ai} = \dot{\boldsymbol{v}}_p + \dot{\omega}_p \times \boldsymbol{a}_i + \omega_p \times (\omega_p \times \boldsymbol{a}_i). \qquad (25)$$

The acceleration of the kinematic joints A_i, in the fixed coordinate system, is also expressed by taking the derivative of (19) with respect to time

$$\dot{v}_{ai} = \ddot{d}_i \boldsymbol{s}_i + 2\dot{d}_i \omega_i \times \boldsymbol{s}_i + d_i \dot{\omega}_i \times \boldsymbol{s}_i + d_i \omega_i \times (\omega_i \times \boldsymbol{s}_i). \quad (26)$$

Taking the dot product of both sides of (25) with s_i,

$$\dot{\omega}_i = \frac{\boldsymbol{s}_i \times \dot{v}_{ai} - 2\dot{d}_i \omega_i}{d_i} = \boldsymbol{J}_w \ddot{\boldsymbol{q}} + \boldsymbol{K}_w \dot{\boldsymbol{q}} \qquad (27)$$

where $\boldsymbol{K}_w = \dfrac{\tilde{\boldsymbol{s}}_i \dot{\boldsymbol{J}}_{ai} - 2\boldsymbol{J}_a \boldsymbol{J}_w \dot{\boldsymbol{q}}}{d_i}$.

Taking the derivative of (17) with respect to time, the acceleration of the active prismatic joint can be obtained as

$$\ddot{d}_i = \boldsymbol{s}_i^{\mathrm{T}} \cdot \dot{v}_{ai} + v_{ai}^{\mathrm{T}} \cdot (\omega_i \times \boldsymbol{s}_i) = \boldsymbol{J}_d \ddot{\boldsymbol{q}} + \boldsymbol{K}_l \dot{\boldsymbol{q}} \qquad (28)$$

where $\boldsymbol{K}_l = \boldsymbol{s}_i^{\mathrm{T}} \cdot \dot{\boldsymbol{J}}_{ai} - [\boldsymbol{J}_{ai} \dot{\boldsymbol{q}}]^{\mathrm{T}} \cdot \tilde{\boldsymbol{s}}_i \cdot \boldsymbol{J}_{wi}$.

The acceleration of the center of mass of the swing rod and the telescopic rod can be obtained by differentiating (13) and (14) with respect to time:

$$\dot{v}_{1i} = e_1 \dot{\omega}_i \times \boldsymbol{s}_i + e_1 \omega_i \times (\omega_i \times \boldsymbol{s}_i) = \boldsymbol{J}_{v1i} \ddot{\boldsymbol{q}} + \boldsymbol{J}_1 \dot{\boldsymbol{q}} \quad (29)$$

where $\boldsymbol{J}_1 = -e_1 \tilde{\boldsymbol{s}}_i \boldsymbol{K}_w - e_1 \boldsymbol{s}_i \cdot (\boldsymbol{J}_{wi} \dot{\boldsymbol{q}})^{\mathrm{T}} \boldsymbol{J}_{wi}$

$$\begin{aligned} \dot{v}_{2i} =& \ddot{d}_i \cdot \boldsymbol{s}_i + 2\dot{d}_i(\omega_i \times \boldsymbol{s}_i) + (d_i - e_2)\dot{\omega}_i \times \boldsymbol{s}_i + \\ & (d_i - e_2)\dot{\omega}_i \times (\omega_i \times \boldsymbol{s}_i) = \\ & \boldsymbol{J}_{v2i} \ddot{\boldsymbol{q}} + \boldsymbol{J}_2 \dot{\boldsymbol{q}} \end{aligned} \qquad (30)$$

and $\boldsymbol{J}_2 = \boldsymbol{s}_i \cdot \boldsymbol{K}_l - 2\boldsymbol{J}_{di} \cdot \dot{\boldsymbol{q}} \cdot \tilde{\boldsymbol{s}}_i \cdot \boldsymbol{J}_{wi} + (e_2 - d_i)[\tilde{\boldsymbol{s}}_i \cdot \boldsymbol{K}_w + \boldsymbol{s}_i(\boldsymbol{J}_{wi} \dot{\boldsymbol{q}})^T \boldsymbol{J}_{wi}]$.

3 Dynamics analysis

The inverse dynamics problem of the parallel manipulator is to determine the required driving force under the requirement to produce output motion trajectory. According to d'Alembert's principle, the force applied on the centroid of each component includes gravity, inertia force and inertia moment. When we considered the whole system, ignoring the effect of friction in the component, the external force and inertia wrenches exerted on the center of the moving platform can be expressed as

$$\boldsymbol{F}_p = \begin{bmatrix} \boldsymbol{f}_p \\ \boldsymbol{n}_p \end{bmatrix} = \begin{bmatrix} \boldsymbol{f}_e + m_a \boldsymbol{g} - m_a \dot{\boldsymbol{v}}_p \\ \boldsymbol{n}_e - {}^B \boldsymbol{I}_p \dot{\omega}_p - \omega_p \times ({}^B \boldsymbol{I}_p \omega_p) \end{bmatrix} \qquad (31)$$

where $\boldsymbol{f}_e$ and $\boldsymbol{n}_e$ represent the external force and the external torque acting at the center of the moving platform, respectively. ${}^B \boldsymbol{I}_p = {}^B \boldsymbol{R}_A {}^A \boldsymbol{I}_p ({}^B \boldsymbol{R}_A)^{\mathrm{T}}$ is the inertia matrix of the moving platform in the fixed coordinate system.

Assuming that the external force acting on the chain is only gravity, the external force and inertia force of the chain in the fixed coordinate system can be expressed as

$$\boldsymbol{F}_{1i} = \begin{bmatrix} \boldsymbol{f}_{1i} \\ \boldsymbol{n}_{1i} \end{bmatrix} = \begin{bmatrix} m_{1i} \boldsymbol{g} - m_{1i} \dot{\boldsymbol{v}}_{1i} \\ -{}^B \boldsymbol{I}_{1i} \dot{\omega}_i - \omega_i \times ({}^B \boldsymbol{I}_{1i} \omega_i) \end{bmatrix} \qquad (32)$$

$$\boldsymbol{F}_{2i} = \begin{bmatrix} \boldsymbol{f}_{2i} \\ \boldsymbol{n}_{2i} \end{bmatrix} = \begin{bmatrix} m_{2i} \boldsymbol{g} - m_{2i} \dot{\boldsymbol{v}}_{2i} \\ -{}^B \boldsymbol{I}_{2i} \dot{\omega}_i - \omega_i \times ({}^B \boldsymbol{I}_{2i} \omega_i) \end{bmatrix} \qquad (33)$$

where ${}^B \boldsymbol{I}_{1i} = {}^B \boldsymbol{R}_i {}^i \boldsymbol{I}_{1i} ({}^B \boldsymbol{R}_i)^{\mathrm{T}}$, ${}^B \boldsymbol{I}_{2i} = {}^B \boldsymbol{R}_i {}^i \boldsymbol{I}_{2i} ({}^B \boldsymbol{R}_i)^{\mathrm{T}}$.

In the above, ${}^i \boldsymbol{I}_{1i}$ and ${}^i \boldsymbol{I}_{2i}$ stand for the inertia matrix of the swing rod and the telescopic rod is expressed in the chain local coordinate system, respectively.

We now adopt the principle of virtual work, and the dynamics equation of the redundantly actuated and overconstrained 2RPU-2SPR parallel manipulator can be expressed as

$$\delta \boldsymbol{d}^{\mathrm{T}} \tau + \delta \boldsymbol{q}^{\mathrm{T}} \boldsymbol{F}_p + \sum_i (\delta \boldsymbol{r}_{1i}^{\mathrm{T}} \boldsymbol{F}_{1i} + \delta \boldsymbol{r}_{2i}^{\mathrm{T}} \boldsymbol{F}_{2i}) = 0. \qquad (34)$$

The virtual displacement in (34) must satisfy the motion constraints of the kinematic joints, therefore, it is necessary to associate the virtual displacement with a series of independent generalized displacement, namely

$$\delta\boldsymbol{d} = \boldsymbol{J}_d\delta\boldsymbol{q} \tag{35}$$

$$\delta\boldsymbol{r}_{1i} = \boldsymbol{J}_{v\omega1}\delta\boldsymbol{q} \tag{36}$$

$$\delta\boldsymbol{r}_{2i} = \boldsymbol{J}_{v\omega2}\delta\boldsymbol{q}. \tag{37}$$

Substituting (35)–(37) into (34) and simplifying yields

$$\boldsymbol{v}_s{}^{\mathrm{T}} \cdot \boldsymbol{J}_p{}^{\mathrm{T}}(\boldsymbol{J}_d{}^{\mathrm{T}}\tau + \boldsymbol{F}_p + \sum_i \boldsymbol{J}_{v\omega1}{}^{\mathrm{T}}\boldsymbol{F}_{1i} + \sum_i \boldsymbol{J}_{v\omega2}{}^{\mathrm{T}}\boldsymbol{F}_{2i}) = 0. \tag{38}$$

For arbitrary v_s, the (38) is always satisfied, hence we can obtain

$$\boldsymbol{J}_p{}^{\mathrm{T}}(\boldsymbol{J}_d{}^{\mathrm{T}}\tau + \boldsymbol{F}_p + \sum_i \boldsymbol{J}_{v1}{}^{\mathrm{T}}\boldsymbol{F}_{1i} + \sum_i \boldsymbol{J}_{v2}{}^{\mathrm{T}}\boldsymbol{F}_{2i}) = 0. \tag{39}$$

Simplifying (39), the driving forces can be obtained as follows:

$$\tau = -\left[(\boldsymbol{J}_d\boldsymbol{J}_p)^{\mathrm{T}}\right]^+ \boldsymbol{J}_p{}^{\mathrm{T}}(\boldsymbol{F}_p + \sum_i \boldsymbol{J}_{v\omega1}{}^{\mathrm{T}}\boldsymbol{F}_{1i} + \sum_i \boldsymbol{J}_{v\omega2}{}^{\mathrm{T}}\boldsymbol{F}_{2i}) \tag{40}$$

where $[\cdot]^+$ denotes the Moore-Penrose inverse matrix. The Moore-Penrose inverse of the matrix $\boldsymbol{J}_0{}^{\mathrm{T}}$ can be denoted as $\left(\boldsymbol{J}_0{}^{\mathrm{T}}\right)^+ = \boldsymbol{J}_0(\boldsymbol{J}_0{}^{\mathrm{T}}\boldsymbol{J}_0)^{-1}$ and the condition $(\boldsymbol{J}_0{}^{\mathrm{T}})^+\boldsymbol{J}_0{}^{\mathrm{T}} = \boldsymbol{E}$ should be satisfied.

Equation (40) is a dynamics model of the parallel manipulator, which can be simplified and the general expression of dynamics equation in the joint space can be written as

$$\tau = \boldsymbol{M}(\boldsymbol{q})\ddot{\boldsymbol{q}} + \boldsymbol{C}(\boldsymbol{q})\dot{\boldsymbol{q}} + \boldsymbol{G}(\boldsymbol{q}) - \left[(\boldsymbol{J}_d\boldsymbol{J}_p)^{\mathrm{T}}\right]^+ \boldsymbol{J}_p{}^{\mathrm{T}} \begin{bmatrix} \boldsymbol{f}_e \\ \boldsymbol{n}_e \end{bmatrix} \tag{41}$$

where

$$\boldsymbol{M}(\boldsymbol{q})\ddot{\boldsymbol{q}} = \left[(\boldsymbol{J}_d\boldsymbol{J}_p)^{\mathrm{T}}\right]^+ \boldsymbol{J}_p{}^{\mathrm{T}}$$
$$\left\{ \begin{bmatrix} m_a\dot{\boldsymbol{v}}_p \\ {}^B\boldsymbol{I}_p\dot{\omega}_P \end{bmatrix} + \sum_i \boldsymbol{J}_{v\omega1i}{}^{\mathrm{T}} \begin{bmatrix} m_{1i}\dot{\boldsymbol{v}}_{1i} \\ {}^B\boldsymbol{I}_{1i}\dot{\omega}_i \end{bmatrix} + \right.$$
$$\left. \sum_i \boldsymbol{J}_{v\omega2i}{}^{\mathrm{T}} \begin{bmatrix} m_{2i}\dot{\boldsymbol{v}}_{2i} \\ {}^B\boldsymbol{I}_{2i}\dot{\omega}_i \end{bmatrix} \right\}$$

$$\boldsymbol{C}(\boldsymbol{q})\dot{\boldsymbol{q}} = \left[(\boldsymbol{J}_d\boldsymbol{J}_p)^{\mathrm{T}}\right]^+ \boldsymbol{J}_p{}^{\mathrm{T}}$$
$$\left\{ \begin{bmatrix} \boldsymbol{0} \\ \omega_P \times ({}^B\boldsymbol{I}_p\omega_P) \end{bmatrix} + \sum_i \boldsymbol{J}_{v\omega1i}{}^{\mathrm{T}} \begin{bmatrix} \boldsymbol{0} \\ \omega_i \times ({}^B\boldsymbol{I}_{1i}\omega_i) \end{bmatrix} + \right.$$
$$\left. \sum_i \boldsymbol{J}_{v\omega2i}{}^{\mathrm{T}} \begin{bmatrix} \boldsymbol{0} \\ \boldsymbol{\omega}_i \times ({}^B\boldsymbol{I}_{2i}\omega_i) \end{bmatrix} \right\}$$

$$\boldsymbol{G}(\boldsymbol{q}) = -\left[(\boldsymbol{J}_d\boldsymbol{J}_p)^{\mathrm{T}}\right]^+ \boldsymbol{J}_p{}^{\mathrm{T}} \left\{ \begin{bmatrix} m_a\boldsymbol{g} \\ \boldsymbol{0} \end{bmatrix} + \sum_i \boldsymbol{J}_{v\omega1}{}^{\mathrm{T}} \right.$$
$$\left. \begin{bmatrix} m_{1i}\boldsymbol{g} \\ \boldsymbol{0} \end{bmatrix} + \sum_i \boldsymbol{J}_{v\omega2}{}^{\mathrm{T}} \begin{bmatrix} m_{2i}\boldsymbol{g} \\ \boldsymbol{0} \end{bmatrix} \right\}$$

where $\boldsymbol{M}(\boldsymbol{q})$ is the generalized inertia matrix of the redundantly actuated and over-constrained parallel manipulator which characterizes the mapping relationship between the acceleration of the moving platform and the actuating torques, $\boldsymbol{C}(\boldsymbol{q})$ is the nonlinear velocity coefficient term including the centripetal force and the Coriolis force, and $\boldsymbol{G}(\boldsymbol{q})$ is the gravitational force term of the inverse dynamic equations.

Because of the coupling characteristics of the mechanism, $\boldsymbol{M}(\boldsymbol{q})\ddot{\boldsymbol{q}}$ can be reorganized to obtain the inertia matrix indicating the acceleration mapping relationship between the joint driving force/torque and the independent motion parameter, namely

$$\boldsymbol{M}(\boldsymbol{v}_s)_{4\times3} = \left[(\boldsymbol{J}_d\boldsymbol{J}_p)^{\mathrm{T}}\right]^+ \left\{ \boldsymbol{J}_p{}^{\mathrm{T}} \begin{bmatrix} m_a\boldsymbol{J}_{vp} \\ {}^B\boldsymbol{I}_p\boldsymbol{J}_{\omega p} \end{bmatrix} + \right.$$
$$\sum_i \boldsymbol{J}_p{}^{\mathrm{T}}\boldsymbol{J}_{v\omega1i}{}^{\mathrm{T}} \begin{bmatrix} m_{1i}\boldsymbol{J}_{v1i} \\ {}^B\boldsymbol{I}_{1i}\boldsymbol{J}_{\omega i} \end{bmatrix} \boldsymbol{J}_p + $$
$$\left. \sum_i \boldsymbol{J}_p{}^{\mathrm{T}}\boldsymbol{J}_{v\omega2i}{}^{\mathrm{T}} \begin{bmatrix} m_{2i}\boldsymbol{J}_{v2i} \\ {}^B\boldsymbol{I}_{2i}\boldsymbol{J}_{\omega i} \end{bmatrix} \boldsymbol{J}_p \right\}. \tag{42}$$

4 Dynamics performance indices

Upon considering the application and working conditions of the parallel manipulator, this paper treats the dynamics dexterity, inertia coupling characteristics, the energy transmission efficiency and the driving force/torque balance as the performance indices of the proposed parallel manipulator.

4.1 Dynamics dexterity

Dynamics dexterity is an important index to evaluate the acceleration and deceleration characteristics of the mechanism. Because the inertia factor related to the acceleration plays a crucial role, the generalized inertia ellipsoid is established based on the generalized inertial ellipsoid principle, and dynamics dexterity index is adopted for evaluating the dynamics performance and inertia characteristics of the mechanism. The ratio of the minimum and maximum singular eigenvalue of the inertia matrix, that is the reciprocal of condition numbers, can be used as the evaluation index

$$k_M = \frac{\lambda_{\min}(\boldsymbol{M})}{\lambda_{\max}(\boldsymbol{M})} \tag{43}$$

when $k_M = 1$, it is shown that the mechanism was dynamics isotropic in this configuration. The dynamics

dexterity k_M satisfies the range of $0 \leq k_M \leq 1$, and when the value of k_M is close to 1, the parallel manipulator has good dynamics dexterity and the acceleration performance.

4.2 Inertia coupling characteristic

The inertia coupling characteristics is the main factor affecting the dynamic response of the parallel manipulator. For the parallel manipulator with rotations and translation coupling degrees of freedom, the coupling characteristics of the inertia force/torque will affect the output precision. Therefore, it is very important to reasonably evaluate the inertia coupling characteristics of the parallel manipulator for eliminating or reducing the errors caused by the inertia coupling[31]. The ratio of the sum of absolute values in every row of the inertia matrix $M(q)$ expect the main diagonal elements and absolute value of the main diagonal elements is employed as the measure index of the coupling magnitude of the coupling inertia and the equivalent inertia of the mechanism, namely

$$MIC_1 = \frac{|M_{12}| + |M_{13}|}{|M_{11}|}$$

$$MIC_2 = \frac{|M_{21}| + |M_{23}|}{|M_{22}|}$$

$$MIC_3 = \frac{|M_{31}| + |M_{32}|}{|M_{33}|} \qquad (44)$$

where MIC denotes the inertia coupling index of the parallel manipulator, and the amplitude represents the inertia coupling intensity. When the index increases, it shows that the coupling inertia of the mechanism becomes larger and the coupling characteristics are enhanced, and the dynamic response characteristics of the mechanism are reduced.

4.3 Energy transmission efficiency

For the parallel manipulator with rotations and translation coupling degrees of freedom, owing to the inconsistent dimension, the algebraic values of condition number or manipulability will present the phenomenon of unknown physical meaning. With introduction of the energy efficiency coefficient, a dimensionless performance index is independent coordinate system, which can be utilized to evaluate the dynamics performance of the parallel manipulator. For parallel manipulator, the output energy of the moving platform is treated as the effective energy, and the ratio of the effective energy to all the energy of storage components is used as the energy transmission efficiency[32, 33], i.e.,

$$\eta = \frac{E_p}{E_{all}} \qquad (45)$$

where E_p is the energy of the moving platform, and E_{all} is the energy of the parallel manipulator, namely

$$E_p = \frac{1}{2} v_s{}^T (m_a J_{vp}{}^T J_{vp} + J_{\omega p}{}^{TB} I_p J_{\omega p}) v_s$$

$$\begin{aligned} E_{all} = &\frac{1}{2} v_s{}^T [m_a J_{vp}{}^T J_{vp} + J_{\omega p}{}^{TB} I_p J_{\omega p} + \\ &\sum_i (m_{1i} J_{v1}{}^T J_{v1} + J_{\omega 1}{}^{TB} I_{1i} J_{\omega 1}) + \\ &\sum_i (m_{2i} J_{v2}{}^T J_{v2} + J_{\omega 2}{}^{TB} I_{2i} J_{\omega 2})] v_s. \end{aligned}$$

Obviously, the higher the energy of the moving platform is, the greater is the energy transmission efficiency.

4.4 Driving force/torque balance

Inspired by the probability theory, this paper undertakes a research on the fluctuation of the discrete points. The concept of driving force/torque mean and deviation are generally used to evaluate driving force/torque balance. The actuation force value at the prismatic joint of each driving chain τ_1, τ_2, τ_3 and τ_4 can be calculated for a given desired task requirement, the driving force mean $\bar{\tau}$ can be straightforwardly expressed as

$$\bar{\tau} = \frac{(\tau_1 + \tau_2 + \tau_3 + \tau_4)}{4}. \qquad (46)$$

And the standard deviation σ of the four driving forces can be calculated, i.e.,

$$\sigma = \sqrt{\frac{(\tau_1 - \bar{\tau})^2 + (\tau_2 - \bar{\tau})^2 + (\tau_3 - \bar{\tau})^2 + (\tau_4 - \bar{\tau})^2}{4}} \qquad (47)$$

where $\bar{\tau}$ denotes the mean index of the driving forces, and σ is the balance stability index of the four driving branches.

5 Application examples and performance analysis

In accordance with specific task requirement, a physical prototype (as depicted in Fig. 4) is fabricated, whose main technical parameters are listed as: the radius of the base is $r_a = 0.15\,\mathrm{m}$, the radius of the moving platform is $r_b = 0.25\,\mathrm{m}$, the mass of the moving platform is $m_a = 5\,\mathrm{kg}$, the mass of the swing rod is $m_{1i} = 2.5\,\mathrm{kg}$, the mass of the telescopic rod is $m_{2i} = 0.5\,\mathrm{kg}$, the distance between the centroid of the swing rod and the universal joint B_i is $e_1 = 0.3\,\mathrm{m}$, the distance between the centroid of the telescopic rod and the joint A_i is $e_2 = 0.2\,\mathrm{m}$, the gravity acceleration is $g = \begin{bmatrix} 0 & 0 & -9.807 \end{bmatrix}^T$, the external force $f_e = \begin{bmatrix} 2 & 5 & 8 \end{bmatrix}^T$ and the external torque

Fig. 4   A physical prototype of the parallel manipulator

$\boldsymbol{n}_e = \begin{bmatrix} 1 & 3 & 5 \end{bmatrix}^{\mathrm{T}}$, and the inertia matrix about the center of mass of chain i can be determined by the Solidworks software as follows (unit: kg·m^2):

$$^A\boldsymbol{I}_p = \begin{bmatrix} 2.3 & 0 & 0 \\ 0 & 4.9 & 0 \\ 0 & 0 & 3.1 \end{bmatrix} \times 10^{-3}$$

$$^i\boldsymbol{I}_{1i} = \begin{bmatrix} 8.3 & 0 & 0 \\ 0 & 8.3 & 0 \\ 0 & 0 & 0.3 \end{bmatrix} \times 10^{-2}$$

$$^i\boldsymbol{I}_{2i} = \begin{bmatrix} 2.2 & 0 & 0 \\ 0 & 2.2 & 0 \\ 0 & 0 & 0.01 \end{bmatrix} \times 10^{-2}.$$

Specifically, the motion trajectory parameter equation of the moving platform is given as

$$\begin{cases} \alpha(t) = \dfrac{\pi}{6}\sin(2t) \\ \beta(t) = \dfrac{\pi}{6}\sin(2t) \\ z = 0.8 + 0.2\sin(2t). \end{cases} \tag{48}$$

5.1   Dynamics dexterity analysis

The results of the analysis are depicted in Fig. 5, where the distribution of dynamics dexterity at different heights is demonstrated. From Fig. 5, the dexterity of the mechanism is closer to 1 as the height decreases, which indicates better dynamics dexterity and higher motion precision of the mechanism. Moreover, the range of the local condition number varies continuously in 0.2–1, and the value decreases when the configuration gets close to
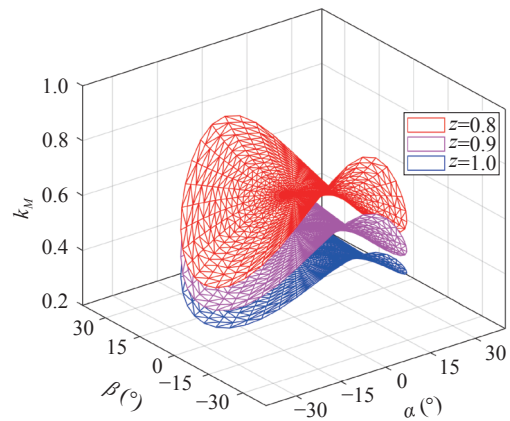
Fig. 5   Distribution of dynamics dexterity at different height (color versions of the figures in this paper are available online)

the boundary of the workspace. Furthermore, the distribution is uniform, the change is stable, and there is no sudden change, which illustrate that the proposed parallel manipulator has better dynamics dexterity.

5.2   Inertia coupling index analysis

Figs. 6–8 show the inertial coupling index distribution atlases of the redundantly actuated and over-constrained 2RPU-2SPR parallel manipulator at different heights.

The variations of the coupling inertia characteristics index of the parallel manipulator are depicted in Figs. 6–8. It is shown in Fig. 6 that the effect of the actuator force, and the value of MIC_1 is little smaller than MIC_2 or MIC_3, which means that the diagonal element is larger than the others, and accounts for the dominant factor of the inertial term. In fact, this also explains (2), $x = 0$, without parasitic motion in x direction, while $y = -ds\alpha$ has parasitic motion in y direction, so the coupling characteristic is relatively larger than MIC_2 or MIC_3. Figs. 7 and 8 reflect the distribution of the inertial coupling index in the whole workspace, and illustrate the influence of Euler angles α and β at different heights.
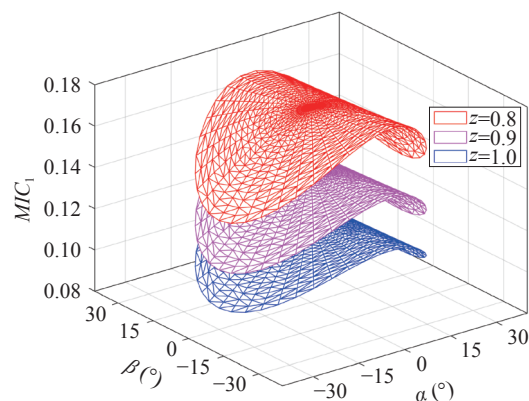

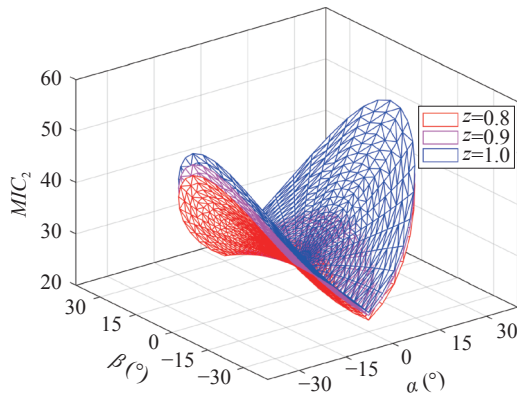Fig. 6   Distribution of MIC_1 versus driving force τ_1

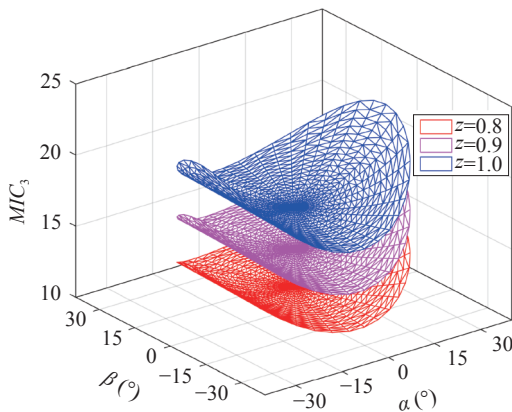Fig. 7   Distribution of MIC_2 versus driving force τ_2

Fig. 8   Distribution of MIC_3 versus driving force τ_3

Owing to the symmetry of the mechanism, the distribution of the inertia coupling index about the coordinate axis also presents certain symmetry. In the whole workspace, Figs. 7 and 8 show that the coupling index of inertia coupling of driving shaft is minimal at the initial position. With the increase of Euler angles α and β, the coupling characteristics is also increasing.

5.3   Energy transmission efficiency analysis

The higher the energy transmission efficiency is, the higher the effective energy of the moving platform is and the lesses the energy loss in the transmission process. If generalized velocity parameter v_s is given, the transmission efficiency of the parallel manipulator can be calculated by (45), and the result can be depicted in Fig. 9.

The range of the energy transmission efficiency index values in whole workspace is 0.705–0.745 according to Fig. 9. Furthermore, the higher the transmission efficiency is, the better transmission performance of the parallel manipulator is. In the path planning of the mechanism, the parallel manipulator should work in the workspace with high energy transmission efficiency as far as possible, so that the mechanism exerts better dynamics performance, simultaneously, the motion precision and
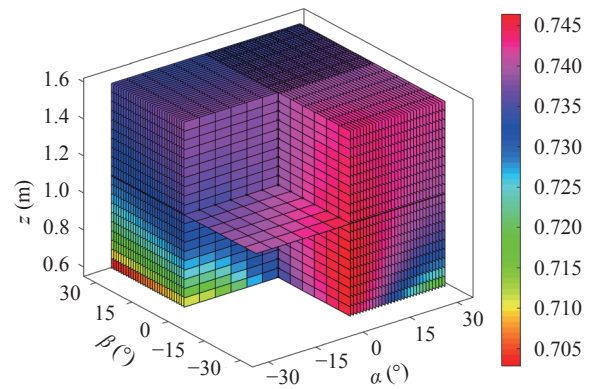

Fig. 9   Distribution of energy transmission efficiency

control precision of the parallel manipulator can be greatly improved by the introduction of actuation redundancy.

5.4   Driving force/torque balance analysis

The distribution of the driving force/torque balance performance index is shown in Fig. 10. According to the given trajectory expression (48), the moving platform conducts certain motion process, the variation range of the mean of the driving force is 0–4. The standard deviation of the driving force changes with 4–16. The changes of mean and the standard deviation of the driving force are continuous, without mutation and jump, which shows that the potential distributions are in the smooth channel and the driving force/torque balance performance of the parallel manipulator is very well.
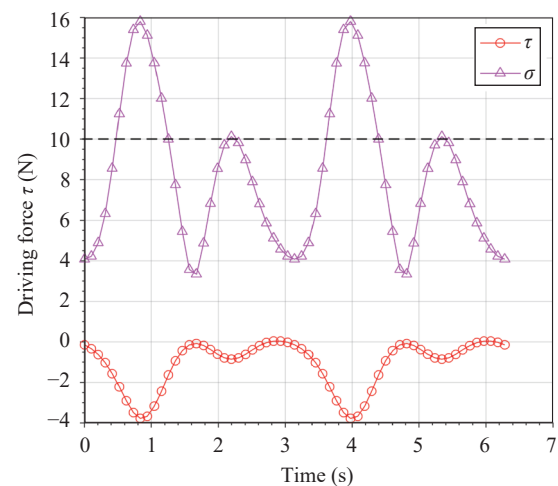

Fig. 10   Driving forces mean and deviation versus time

The amplitude of the required driving force of the redundantly actuated and over-constrainted 2RPU-2SPR parallel manipulator is shown in Fig. 11. It is obvious that the driving force of the servomotor is changed smoothly under the external force and torque, without singularity and mutation, which embodies the superior dynamics per-

formance of the parallel manipulator, and the driving force curves τ_1 and τ_3, curves τ_2 and τ_4 are approximately symmetric, for which the driving force behavior is not only affected by the structural parameters of itself, but also affected by the parasitic motion characteristics (seen from (2) and (3)).

The four driving forces of the redundantly actuated and over-constrained 2RPU-2SPR parallel manipulator with respect to time are achieved and shown in Fig. 11. It is worth noting that the maximum driving force of the whole motion process is 42.4 N under the prescribed motion trajectory. Under the same motion trajectory and the same structural parameters, the three driving forces of the non-redundant over-constrained 2RPU-SPR parallel manipulator, removing the fourth SPR limb, are plotted in Fig. 12. The maximum value of the driving force is 51.6 N. By contrast, with the introduction of actuation redundancy, the maximum driving force of the redundantly actuated parallel manipulator is less than non-re-

Fig. 11 Driving forces of redundantly actuated parallel manipulator

Fig. 12 Driving forces of non-redundantly actuated parallel manipulator

dundant parallel manipulator, which shows that the redundant actuation can effectively decrease the driving force and improve the dynamics comprehensive performance of the mechanism.

6 Conclusions

In this paper, the dynamics performance evaluation method for a novel redundantly actuated and over-constrained 2RPU-2SPR parallel manipulator with two rotations and one translation coupling degrees of freedom is systematically investigated, and the following conclusions can be obtained:

1) The inverse position analysis of the proposed parallel manipulator has been formulated, and the mapping relationship of velocity and acceleration between the driving chain and operating joint space are straightforwardly deduced. In terms of the principle of virtual work, the dynamics standard formulation of the proposed parallel manipulator is established and the inertia matrix including acceleration term is also separated and the optimal driving force value is obtained by employing the generalized Moore-Penrose inverse matrix.

2) The performance evaluation indices including the dynamics dexterity, the inertia coupling characteristics, the energy transmission efficiency, and driving force/ torque balance are introduced. The distribution atlases of the redundantly actuated and over-constrained 2RPU-2SPR parallel manipulator in the workspace are depicted in details. The results show that the proposed mechanism has better dynamics comprehensive performance.

3) The dynamics performance evaluation indices proposed in this paper can well describe the dynamics comprehensive performance of the parallel manipulator, furthermore this study not only provides the theoretical foundation for structure design, trajectory planning and real-time control of the parallel manipulator, but also this parallel manipulator demonstrates a good engineering application prospect.

Acknowledgments

References

[1] M. Mazare, M. Taghizadeh, M. R. Najafi. Kinematic analysis and design of a 3-DOF translational parallel robot. *International Journal of Automation and Computing*, vol. 14, no. 4, pp. 432–441, 2017. DOI: 10.1007/s11633-017-1066-y.

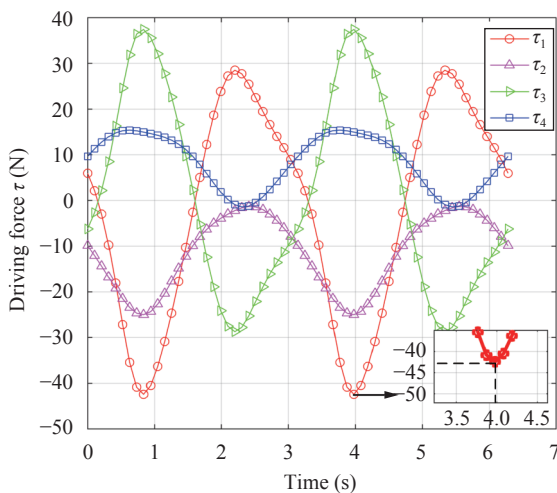[2] B. Siciliano. The Tricept robot: Inverse kinematics, ma-

nipulability analysis and closed-loop direct kinematics algorithm. *Robotica*, vol. 17, no. 4, pp. 437–445, 1999. DOI: 10.1017/S0263574799001678.
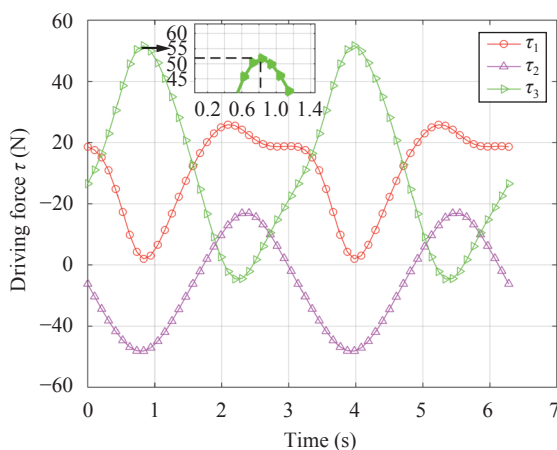
[3]   Z. M. Bi, Y Jin. Kinematic modeling of Exechon parallel kinematic machine. *Robotics and Computer-integrated Manufacturing*, vol. 27, no. 1, pp. 186–193, 2011. DOI: 10.1016/j.rcim.2010.07.006.

[4]   N. Hennes, D. Staimer. Application of PKM in aerospace manufacturing-high performance machining centers ECO-SPEED, ECOSPEED-F and ECOLINER. In *Proceedings of 4th Chemnitz Parallel Kinematics Seminar*, Chemnitz, Germany, pp. 557–577, 2004.

[5]   D. Zhang. *Parallel Robotic Machine Tools*. Boston, USA: Springer, 2010. DOI: 10.1007/978-1-4419-1117-9.

[6]   D. S. Zhang, Y. D. Xu, J. T. Yao, Y. S. Zhao. Inverse dynamic analysis of novel 5-DoF hybrid manipulator. *Transactions of the Chinese Society for Agricultural Machinery*, vol. 48, no. 9, pp. 384–391, 2017. DOI: 10.6041/j.issn.1000-1298.2017.09.049. (in Chinese)

[7]   L. Carbonari. Simplified approach for dynamics estimation of a minor mobility parallel robot. *Mechatronics*, vol. 30, pp. 76–84, 2015. DOI: 10.1016/j.mechatronics.2015.06.005.

[8]   S. Staicu. Dynamics analysis of the Star parallel manipulator. *Robotics and Autonomous Systems*, vol. 57, no. 11, pp. 1057–1064, 2009. DOI: 10.1016/j.robot.2009.07.005.

[9]   Y. M. Li, S. Staicu. Inverse dynamics of a 3-PRC parallel kinematic machine. *Nonlinear Dynamics*, vol. 67, no. 2, pp. 1031–1041, 2011. DOI: 10.1007/s11071-011-0045-z.

[10] H. Abdellatif, B. Heimann. Computational efficient inverse dynamics of 6-DOF fully parallel manipulators by using the Lagrangian formalism. *Mechanism and Machine Theory*, vol. 44, no. 1, pp. 192–207, 2009. DOI: 10.1016/j.mechmachtheory.2008.02.003.

[11] Y. M. Li, Q. S. Xu. Kinematics and inverse dynamics analysis for a general 3-prs spatial parallel mechanism. *Robotica*, vol. 23, no. 2, pp. 219–229, 2005. DOI: 10.1017/S0263574704000797.

[12] Y. W. Li, J. S. Wang, X. J. Liu, L. P. Wang. Dynamic performance comparison and counterweight optimization of two 3-DOF parallel manipulators for a new hybrid machine tool. *Mechanism and Machine Theory*, vol. 45, no. 11, pp. 1668–1680, 2010. DOI: 10.1016/j.mechmachtheory.2010.06.009.

[13] B. Dasgupta, P. Choudhury. A general strategy based on the Newton-Euler approach for the dynamic formulation of parallel manipulators. *Mechanism and Machine Theory*, vol. 34, no. 6, pp. 801–824, 1999. DOI: 10.1016/S0094-114X(98)00081-0.

[14] S. A. A. Moosavian, A. Pourreza, K. Alipour. Dynamics and stability of a hybrid serial-parallel mobile robot. *Mathematical and Computer Modelling of Dynamical Systems*, vol. 16, no. 1, pp. 35–56, 2010. DOI: 10.1080/13873951003676518.

[15] B. Dasgupta, T. S. Mruthyunjaya. Closed-form dynamic equations of the general Stewart platform through the newton-Euler approach. *Mechanism and Machine Theory*, vol. 33, no. 7, pp. 993–1012, 1998. DOI: 10.1016/S0094-114X(97)00087-6.

[16] Y. Yun, Y. M. Li. Design and analysis of a novel 6-DOF redundant actuated parallel robot with compliant hinges for high precision positioning. *Nonlinear Dynamics*, vol. 61, no. 4, pp. 829–845, 2010. DOI: 10.1007/s11071-010-9690-x.

[17] T. Yoshikawa. Dynamic manipulability of robot manipulators. In *Proceedings of IEEE International Conference on Robotics and Automation*, St. Louis, USA, pp. 1033–1038, 1985. DOI: 10.1109/ROBOT.1985.1087277.

[18] H. Asada. Dynamic analysis and design of robot manipulators using inertia ellipsoids. In *Proceedings of IEEE International Conference on Robotics and Automation*, Atlanta, USA, pp. 94–102, 1984. DOI: 10.1109/ROBOT.1984.1087211.

[19] J. Wu, Y. Gao, B. B. Zhang, L. P. Wang. Workspace and dynamic performance evaluation of the parallel manipulators in a spray-painting equipment. *Robotics and Computer-Integrated Manufacturing*, vol. 44, pp. 199–207, 2017. DOI: 10.1016/j.rcim.2016.09.002.

[20] G. H. Cui, D. Zhang, H. D. Zhou, Y. W. Zhang. Operating dexterity optimization and analysis of a 3-DOF parallel manipulator for a tunnel segment assembly system. *International Journal of Mechanics and Materials in Design*, vol. 11, no. 3, pp. 277–285, 2015. DOI: 10.1007/s10999-014-9268-8.

[21] J. Zhang, J. S. Dai, T. Huang. Characteristic equation-based dynamic analysis of a three-revolute prismatic spherical parallel kinematic machine. *Journal of Computational and Nonlinear Dynamics*, vol. 10, no. 2, Article Number 021017, 2015. DOI: 10.1115/1.4028416.

[22] S. Lu, Y. M. Li. Dynamic dexterity evaluation of a 3-DOF 3-PUU parallel manipulator based on generalized inertia matrix. In *Proceedings of IEEE International Conference on Robotics and Biomimetics*, Zhuhai, China, pp. 1506–1511, 2016. DOI: 10.1109/ROBIO.2015.7418984.

[23] M. Li, T. Huang, J. P. Mei, X. M. Zhao, D. G. Chetwynd, S. J. Hu. Dynamic formulation and performance comparison of the 3-DOF modules of two reconfigurable PKM – the tricept and the TriVariant. *Journal of Mechanical Design*, vol. 127, no. 6, pp. 1129–1136, 2005. DOI: 10.1115/1.1992511.

[24] Y. J. Zhao. Dynamic optimum design of a three translational degrees of freedom parallel robot while considering anisotropic property. *Robotics and Computer-Integrated Manufacturing*, vol. 29, no. 4, pp. 100–112, 2013. DOI: 10.1016/j.rcim.2012.11.004.

[25] J. Wu, J. S. Wang, L. P. Wang, T. M. Li. Dynamic formulation of redundant and nonredundant parallel manipulators for dynamic parameter identification. *Mechatronics*, vol. 19, no. 4, pp. 586–590, 2009. DOI: 10.1016/j.mechatronics.2009.01.003.

[26] Y. J. Zhao, K. Qiu, S. X. Wang, Z. Q. Zhang. Inverse kinematics and rigid-body dynamics for a three rotational degrees of freedom parallel manipulator. *Robotics and Computer-Integrated Manufacturing*, vol. 31, pp. 40–50, 2015.

DOI: 10.1016/j.rcim.2014.07.002.

[27] Z. M. Chen, X. M. Liu, Y. Zhang, K. Huang, Z. Huang. Dynamics analysis of a symmetrical 2R1T 3-UPU parallel mechanism. *Journal of Mechanical Engineering*, vol. 21, pp. 46–53, 2017. (in Chinese)

[28] Y. Jiang, T. M. Li, L. P. Wang. Dynamic modeling and redundant force optimization of a 2-DOF parallel kinematic machine with kinematic redundancy. *Robotics and Computer-Integrated Manufacturing*, vol. 32, pp. 1–10, 2015. DOI: 10.1016/j.rcim.2014.08.001.

[29] H. Q. Zhang, H. R. Fang. Stiffness characteristics analysis of a novel 3-DOF parallel kinematic machine tool. *International Journal of Engineering and Technology*, vol. 10, no. 4, pp. 346–354, 2018. DOI: 10.7763/IJET.2018.V10.1082.

[30] H. Ming, J. S. Shun. The kinematic analyses of the 3-DOF parallel machine tools. *International Journal of Automation and Computing*, vol. 8, no. 1, pp. 107–111, 2011. DOI: 10.1007/s11633-010-0561-1.

[31] D. Wang, J. Wu, L. P. Wang, X. J. Liu. Research on the inertia coupling property of a 3-PRS parallel robot. *Chinese Journal of Theoretical and Applied Mechanics*, vol. 48, no. 4, pp. 804–812, 2016. DOI: 10.6052/0459-1879-16-160. (in Chinese)

[32] B. B. Zhang, L. P. Wang, J. Wu. Dynamic isotropic performance evaluation of a 3-DOF parallel manipulator. *Journal of Tsinghua University* (*Science and Technology*), vol. 57, no. 8, pp. 803–809, 2017. DOI: 10.16511/j.cnki.qh-dxxb.2017.22.041. (in Chinese)

[33] H. E. Ghor, E. M. Aggoune. Energy efficient scheduler of aperiodic jobs for real-time embedded systems. *International Journal of Automation and Computing*, 2016. DOI: 10.1007/s11633-016-0993-3.

Hai-Qiang Zhang received the B. Eng. degree in mechanical design and theories from Yantai University, China in 2012, the M. Eng. degree in mechanical engineering from Hebei University of Engineering, China in 2015. He is a Ph. D. degree candidate at Beijing Jiaotong University, China.

His research interests include robotics in computer integrated manufacturing, parallel kinematics machine tool, redundant actuation robots, over-constrained parallel manipulators, and multi-objective optimization design.

E-mail: 16116358@bjtu.edu.cn

ORCID iD: 0000-0003-4421-5671

Hai-Rong Fang received the B. Eng. degree in mechanical engineering from Nanjing University of Science and Technology, China in 1990, the M. Eng. degree in mechanical engineering from Sichuan University, China in 1996, and the Ph. D. degree in mechanical engineering from Beijing Jiaotong University, China in 2005. She worked as associate professor in Department of Engineering Mechanics at Beijing Jiaotong University, China, from 2003 to 2011. She is a professor in School of Mechanical Engineering from 2011 and director of Robotics Research Center.

Her research interests include parallel mechanisms, digital control, robotics and automation, machine tool equipment.

E-mail: hrfang@bjtu.edu.cn (Corresponding author)

ORCID iD: 0000-0001-7938-4737
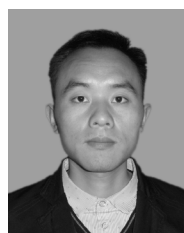
Bing-Shan Jiang received the B. Eng. degree in mechanical electronic engineering from Liaoning Technical University, China in 2015, and the M. Eng. degree in mechanical engineering from Liaoning Technical University, China in 2017. He is currently a Ph. D. degree candidate at School of Mechanical, Electronic and Control Engineering, Beijing Jiaotong University, China.

His research interests include synthesis, kinematics, dynamics and control of parallel robots.

E-mail: 17116381@bjtu.edu.cn

Shuai-Guo Wang received the B. Eng. degree in mechanical engineering and automation from Changchun University of Technology, China in 2015. He is currently an engineer who works at MH Robot and Automation Limited Company.

His research interests include principle and method of automatic control, automation unit technology and integration technology and its application in all kinds of control systems, robot system integration, and automobile automatic production line.

E-mail: 13336362653@163.com